JOURNAL OF MATERIALS SCIENCE: 30 (1995) 235–242

Mode I fracture behaviour of concrete under biaxial loading

E. K. TSCHEGG, M. ELSER
Institute of Applied and Technical Physics, Technical University Vienna, Austria
H. KREUZER
Consulting Engineer, CH-5605 Dottikon, Bachstr. Switzerland

Most concrete structures are biaxially loaded when cracking occurs and propagates. A test equipment was developed to evaluate fracture mechanic parameters of concrete, based on the principle of wedge splitting. Notched cubic specimens are tested under stable crack propagation. An additional compressive load application device simulates a homogeneous biaxial state of stress. A force–crack opening displacement diagram is obtained from which the specific fracture energy is calculated. The strain softening behaviour is then evaluated by means of numerical modelling. The approach was applied for biaxially loaded concrete samples with 8, 16 and 32 mm maximum size aggregate (MSA). Based on the experimental data a model is developed and discussed. It is found that the fracture energy changes non-uniformly with increasing compressive stress level, and that interaction of microcracking and aggregate interlocking influences the fracture mechanism.

1. Introduction

Civil structures, made of concrete, are generally under a multiaxial state of stress. This is particularly the case for mass concrete structures, such as dams and off-shore structures, and for underground works. For them, knowledge of the material behaviour under usual and unusual loading is of the essence.

Among the many parameters commonly used for material characterization, fracture behaviour has lately become increasingly important. Although a large number of experimental data are available from multiaxial tests on unnotched specimens, most wedge splitting tests are made under uniaxial loading. Among the former, extensive work on cubic specimens, are reported in [1–5], tested cylinders; more recent examples are reported by [6–9].

Several fracture zones may develop when testing unnotched specimens. This certainly influences the observed deformation response, and it is difficult to decide if the response corresponds to a real material property or to an interaction of several fracture zones. The testing of notched specimens avoids this ambiguity, as only one fracture zone develops. This is of particular interest for the numerical evaluation of experimental data where a structural response is considered to be a real material property.

Biaxial test results on notched specimen are rarely found in the literature. Zielinsky [10] investigated the influence of loading rate on stress–strain behaviour under biaxial compressive and impact loading with the split-Hopkinson bar technique using double-notched specimens. A similar technique was used by Weerheijm and co-workers [11, 12] to investigate the influence of rate effect on the pre and post-peak behaviour for several types of concrete.

The present paper describes the fracture behaviour of concrete under a biaxial compressive tensile state of stress applied on notched cubes, see Fig. 1. Concrete, with three distinct maximum size aggregates (MSAs) is investigated under quasi-static loading. Some preliminary results are reported in [13, 14].

2. Experimental procedure

The choice of specimen and the construction of the load application device [15] is novel, because it seems impractical to extend the approach of the RILEM (Réunion Internationale des Laboratores d' Essaiset de Recherches sur les Matériaux et les Constructions.) draft recommendation 50-FMC [16] to biaxial loading. The wedge splitting approach was therefore chosen, as developed by Tschegg [17–19]. This approach has several advantages as compared to the RILEM three point bend test and has therefore also been used by other research groups [20–22].

The basic setup for biaxial loading is the wedge splitting test equipment, according to [17, 18], for conventional uniaxial application, as shown in Fig. 2. Some relevant features are listed below:

1. The specimens are cubes, cylinders or drill cores; they can be machined easily and inexpensively for convenient handling during the experiments. The ratio of specimen weight and ligament area is favourable in comparison with specimens recommended by the RILEM committee [16].

0022–2461

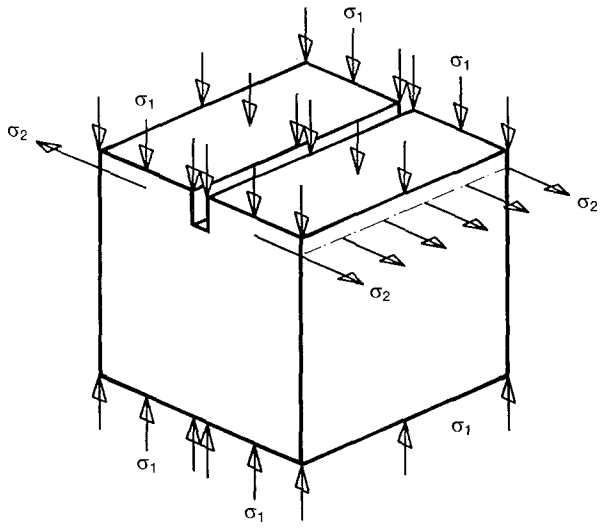

Figure 1 Loading condition of specimen: σ_1, compression stress; σ_2, tension stress and splitting force, respectively.

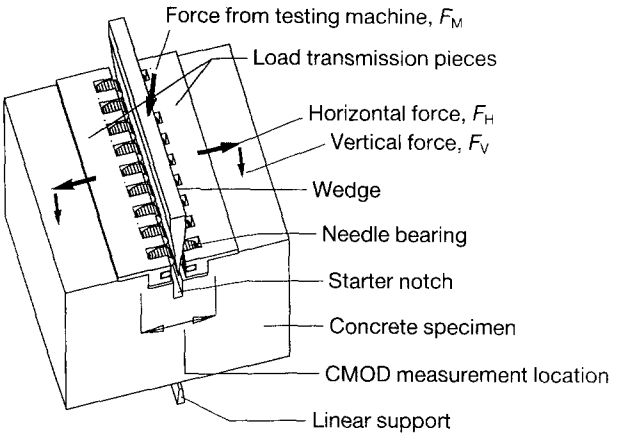

Figure 2 Perspective view of splitting method [16] with notched cubic specimens.

2. Cracking by wedge splitting seems to simulate realistically the mode of surface cracking in concrete parts, e.g. dams and similar structures, due to loadings common in mass concrete structures.

3. The simple and stiff loading equipment allows determination of the full load–deformation curve at surprisingly stable crack growth on large size specimens.

4. A 5–15° wedge is connected to a pressure cell and loaded by a testing machine. It provides the horizontal splitting force, (F_H). The vertical force, (F_V) is small due to the small wedge angle, and influences the result in a negligible manner only [23].

5. The load transfer is direct along the entire notch length and quasi-frictionless via roller bearings. The error of measurement was determined experimentally and is approximately 1% thus being negligible [23].

6. The crack mouth opening displacement (CMOD) is measured by two electronic displacement gauges on both ends of the starter notch at the height of the splitting force. The CMOD measurement unit is separated from the two loading devices and connected to the specimen at a level close to the tip of the starter notch in order to eliminate the measurement of spurious boundary effects.

7. As the loading equipment is very stiff, fracture tests can be performed flawless under stable crack propagation with mechanical or hydraulic machines under "stroke" or "strain" control.

More details on the wedge splitting method, loading and handling equipments may be found in [17–19, 23].

The biaxial state of stress, σ_1 and σ_2, is created by a vertical compressive force and by the horizontal splitting force, F_H, see Figs 1 and 3. Constant and uniform vertical compression is achieved by two symmetric loading frames; each of them are completely separated from the starter notch. They consist of screws, for loading, and stiff transmission slabs. The concrete surface must be ground and parallel to the slabs in order to avoid non-uniform load transmittal. The screws are equipped with strain gauges in order to measure uniform loading for each screw. σ_1 loading has to be applied in small ultimate load increments of 5–10% in order to minimize bending and torsional moments which might cause local premature cracking.

Two aspects of σ_1 loading will be given special attention in the following.

2.1. Homogeneous σ_1 distribution in the specimen

An ideal distribution is achieved if the cube is loaded by two slabs of infinite stiffness. In order to come close to this condition, stress distributions were calculated for several load application devices using the FE (Finite Element) code ABAQUS, see [13, 15]. A linear–elastic three-dimensional analysis for σ_1 loadings between 20 and 80% of the compressive concrete strength was performed, modelling both the cube and all elements of the load application device. The results were used to improve the device until the σ_1 distribution around the fracture process zone was uniform by a margin of less than 3%. Maximum scatter of σ_1 distribution elsewhere was less than 10%, which was considered satisfactory too.

Another possibility to check for a uniform σ_1 loading are pressure measurement films (pre scale-films); these are placed between the sample and the loading slab and discolour when loaded irregularly. A good agreement was found between the analytical and these experimental results. For a detailed description see [15].

Loading in excess of $\sigma_1 = 0.5 f_c$ (f_c = uniaxial compressive strength) would probably cause stress relaxation in the concrete, which, in turn, would then lead to unacceptable stress redistribution due to the stiff load application device. To counteract this phenomenon, springs were inserted into the screws in order to offset some of the relaxation effects, see Fig. 3.

2.2. Balancing lateral strain of concrete and steel

Different Poisson's ratios between concrete and steel leads to an uncontrollable, multiaxial stress distribution at the interface between loading slab and sample. Several solutions are employed to mitigate this problem. In [1] brush bearing plates were recommended

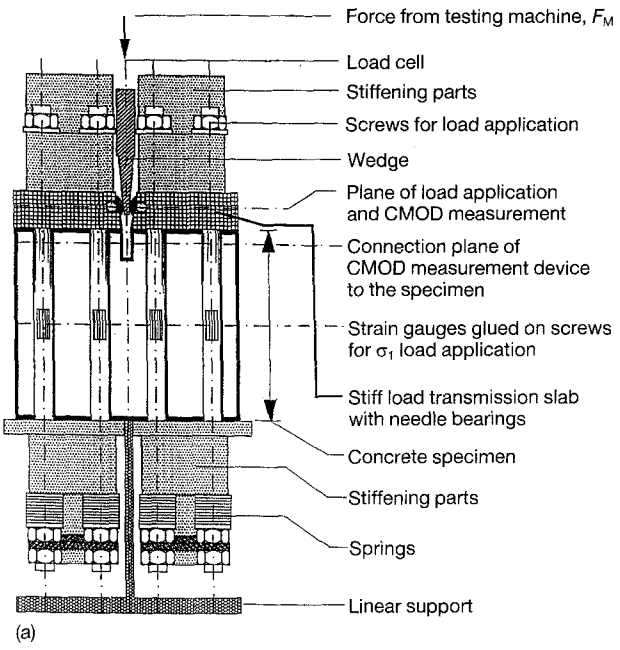

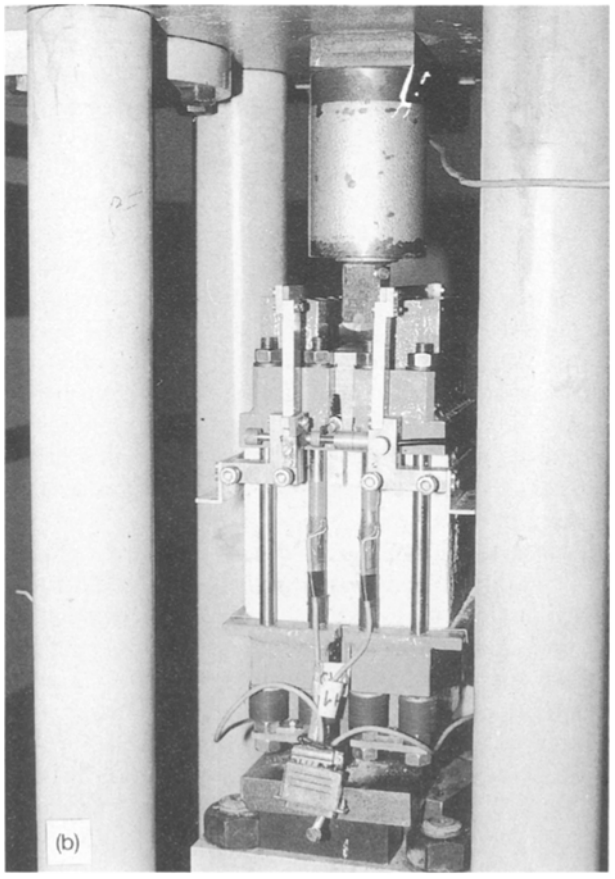

Figure 3 (a) Section through load equipment (wedge splitting equipment plus biaxial compressive loading equipment plus specimen) to produce a defined homogeneous biaxial stress condition. (b) Test facility (specimen, wedge splitting device, biaxial equipment, load displacement measuring device), shown as mounted in the testing machine.

and are commonly accepted now. Another possibility is the use of Teflon plates between loading plate and sample. Both techniques serve the purpose to compensate for the difference in lateral strain between the two materials by reducing the friction coefficient, as extensively discussed in [1]. It is, for example, not sufficient to just grease the interface, which still would give a friction coefficient of 0.3. The use of Teflon plates would reduce friction to 0.02–0.03. This is considered to be a sufficiently low value to compensate for the lateral strain difference. The Teflon plates have the additional advantage that no compressive stress drop has been observed at the boundaries, as experienced with brush bearing plates.

Teflon plates were used in the present progamme. They are inexpensive and do not need much space. Sliding along the loading plate, due to the horizontal splitting force, has been prevented by two 0.5 m deep grooves (rectangular to the loading direction) milled into the plate. This proved to be sufficient, as in no case has sliding been observed.

The simple structure of the biaxial loading device is particularly practical for cubic specimens, easy to operate (no jacks are needed) and inexpensive to acquire. A recent improvement is worked out, in which the manual σ_1 application by torque wrenches, is replaced by a hydraulic jack. This not only improves the loading procedure, but also the pressure regime of σ_1. Details of this equipment is reported in [24].

3. Test programme

The principal objective of the programme was to investigate the fracture response of concrete with different MSAs under biaxial loading. Three mix designs were selected with 8, 16 and 32 mm MSA, respectively, at equal uniaxial compressive strengths of 22 N mm^{-2}, Table I. The ligament length for all 15 cm cubes was 10 cm, resulting in a ligament area of 150 cm^2, Fig. 4.

The cubes were sawn from 64 cm long prisms, with the placing of concrete, perpendicular to the σ_1 direction. Curing was 28 days in water. The starter notch was sawn with a 3 mm thick blade.

σ_2 loading was by a 20 t mechanical testing machine with a crosshead speed of 0.5 mm min^{-1}, corresponding to RILEM recommendations [16]. A 5° wedge angle was used. σ_1 loading was 25, 40/50, 60 and 70/80% of the uniaxial compressive strength.

TABLE I Concrete properties

Property	Maximum size aggregate (mm)		
	8	16	32
Type of aggregate	Rounded limestone and graywacke		
Cement content (kg m^{-3})	3000	260	240
Water–cement ratio	0.73	0.73	0.73
Density (kg m^{-3})	2370	2400	2440
Air content (%)	2.0	1.6	1.1
Compressive cube strength, f_c 28 days (N mm^{-2}) Coefficient of variation ($n = 3$)	21.4	22.0	23.7
Uniaxial tensile strength, f_t 28 days, 50 mm cores (N mm^{-2}) Coefficient of variation ($n = 4$ and 8)	2.1	1.8	1.7
Young's modulus (GPa)	Approx. 25		

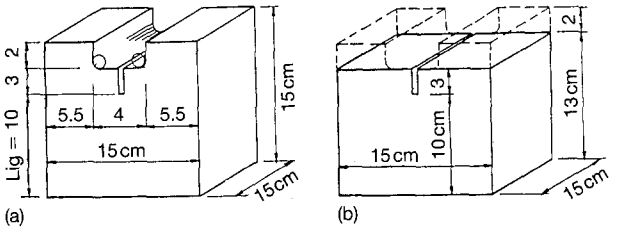

Figure 4 Shape and size of specimens for (a) uniaxial test, and (b) for biaxial test (note that ligament length and area are identical for both specimen shapes).

Three cubes were tested for each of these loading ranges. No unstable material softening was experienced during the entire experimental investigation.

The specific fracture energy, G_f, was chosen as the basic fracture parameter for the following discussion of the experimental results. Its definition and determination follows the RILEM draft recommendations, [16], adapted for wedge splitting testing

$$G_f = \frac{W_0}{A_{lig}} (\mathrm{N\,m^{-1}}).$$

where W_0 is the total fracture energy, which is necessary to completely separate the specimen (this fracture energy is proportional to the area under the load F_H–displacement curve); and A_{lig} is the area of the ligament; where $A_{lig} = 100 \times 150\ \mathrm{mm} = 15\ \mathrm{mm}^2$.

W_0 is derived from the plotted curves, as shown by the examples of Fig. 5, by relating the vertical machine force, F_V, and the horizontal splitting force, F_H

$$F_H = \frac{F_V}{2\tan\alpha}, \qquad \alpha = 5^\circ \text{ wedge angle}$$

The average of the two softening curves (CMOD1–F_V and COMD2–F_V) were used to calculate G_f. If the difference between the two G_f values was in excess of 20% the test was rejected.

4. Results

The measured load–deformation curves show different load peaks and post-peak behaviours for each particular σ_1 loading, which demonstrates the influence of biaxial loading on the extent of damage and fracture modes. A representative case is shown on Fig. 5: with increasing σ_1 loading the load peak decreases, whereas the softening curve flattens. A similar trend, although not as pronounced, is found for the 8 and 16 mm MSA samples.

The same basic findings are demonstrated in Figs 6 and 7 in the form of the G_f–(σ_1/f_C) and (G_f/G_{f_0})–(σ_1/f_C) relations, with σ_1 normalized by the corresponding uniaxial compressive strength, f_C, and G_f by the uniaxial specific fracture energy, G_{f_0}, respectively. It is interesting to note that this relation is not steady. For all mixes a minimum G_f value appears for σ_1 equal to 30–40% of f_c, and from there on the fracture energy increases.

From analogy with classical prepeak relations in the tensile–compression range, one would not expect this kind of unsteady relation. As a matter of fact,

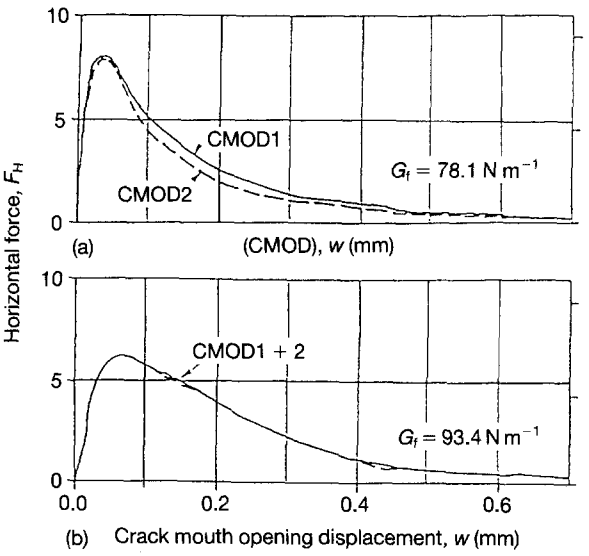

Figure 5 Load–deformation curves of concrete with 32 MSA at a σ_1 load with (a) 25 and (b) 70% compressive strength.

plotting the normalized tensile peak stress, σ_{2max}/f_c, as derived from the peak splitting force, F_H, against σ_1, the well known biaxial envelope shape is obtained, Fig. 8. This relation supports the previously mentioned findings by Kotsovos and Newman [26] and Zielinski [10] who found constant tensile strength (strain) values up to a high compressive stress level. Contrary to this, a continuous decrease of tensile stress with increasing compression has been observed in previous works [e.g. 1–4] with unnotched specimens. More experimental and theoretical studies are necessary in order to investigate if this different behaviour is caused by the use of notched or unnotched specimens or by the use of notched or unnotched specimens, or by the formation of only one or several fracture process zones.

Fractographic studies showed that the development of a fracture surface does not significantly differ for high and low σ_1/f_c values. A statistical evaluation shows a somewhat higher number of transcrystalline grain fractures for high σ_1/f_c values. This effect is more pronounced for MSA 36 mm than for MSA 8 and 16 mm. A qualitative interpretation of the fracture surface roughness shows that it is highest for uniaxial testing and lowest for high σ_1 loading.

5. Discussion

In principle, the fracture energy depends on the material properties prior to loading and on the degree of predamage prior to splitting. They define the extent and shape of the fracture process zone (FPZ). According to Hillerborg *et al.* fictitious crack model [27], the fracture energy is composed of two distinct energy dissipation processes, namely "microcracking" in front of, and "bridging" behind the FPZ. The latter is a frictional energy dissipation process of debonding the aggregates from the matrix, also called aggregate interlock.

The unsteady behaviour as shown in Figs 5, 6 and 9, may be interpreted by a phenomenological way with

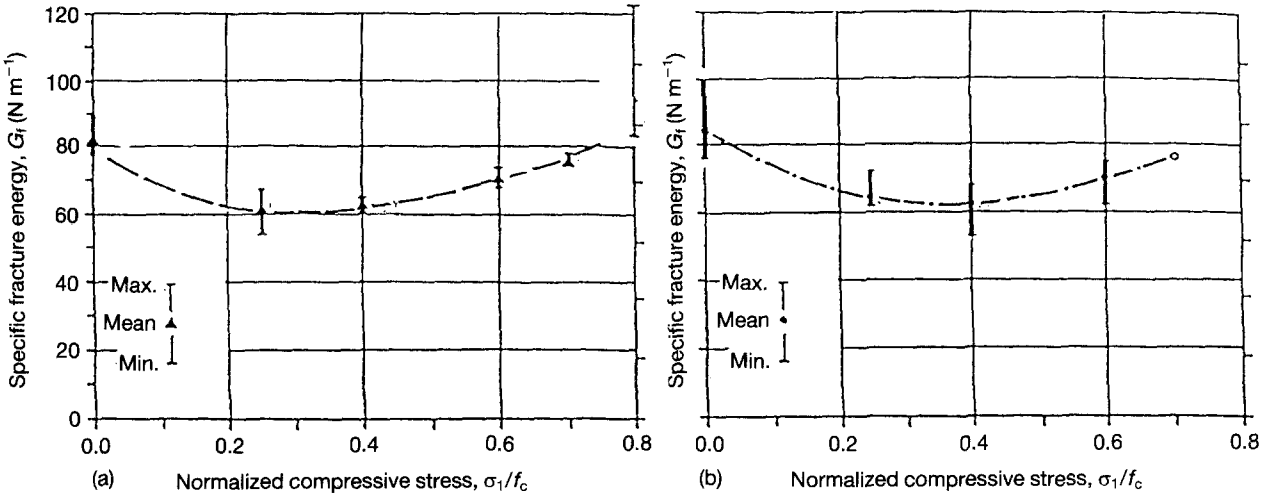

Figure 6 Influence of compression load, σ_1, on the specific fracture energy, G_f, with MSA (a) 8 mm, (b) 16 mm, (c) 32 mm.

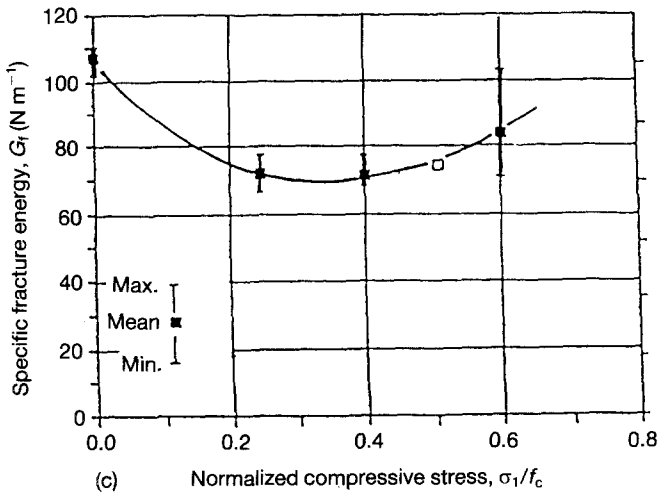

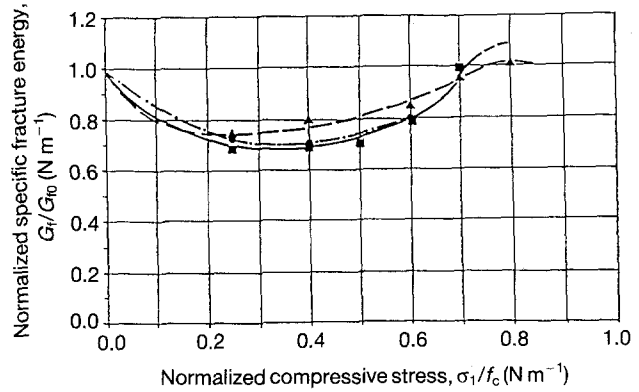

Figure 7 Results of Fig. 6 with normalized fracture energy, G_f/G_{f0} versus σ_1/f_c. For: (▲) MSA = 8 mm, G_f = 82.7 Nm^{-1}; (●) MSA = 16 mm, G_f = 88.2 Nm^{-1}; (■) 32 MSA, G_f = 107.6 Nm^{-1}.

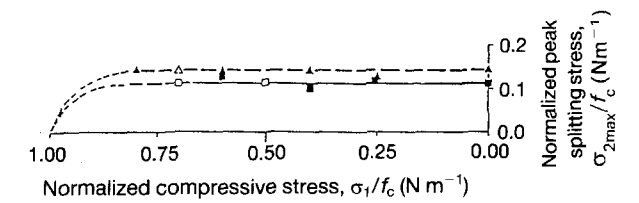

Figure 8 Envelope of the normalized peak-splitting stress σ_{2max}/f_c and compressive stress σ_1/f_c: (– – –) 8 mm MSA; (——) 32 mm MSA; (□, ▽) single values.

the following model, which includes the above two energy dissipating mechanisms. The model is shown in Fig. 9a.

For uniaxial loading ($\sigma_1 = 0$), the FPZ develops at the notch root unimpeded by biaxial loading, as shown schematically in Fig. 9a. Specific fracture energy values, G_{f0} in the range 80 Nm^{-1} are obtained, which increase with increasing MSA owing to the higher "bridging" potential of larger grains.

A biaxial state of stress in the specimen, as long as it remains elastic ($\sigma_1 < 0.4 f_c$), influences the formation of the FPZ. The FPZ becomes narrower and smaller, (Fig. 9b), as the formation of microcracks in a horizontal direction is impeded, or existent microcracks are closed. Contrary to this, vertical microcracks are opened and thus their propagation, or the initiation of microcracks by the splitting force, becomes easier in a vertical direction. A smaller FPZ and less main crack branches (crack path becomes less tortuous) lead to a decrease of the specific fracture energy (zone A in Fig. 9). The "microcracking" part becomes smaller in zone A, whereas the "bridging" part remains constant, as the inner compound is not disturbed, so that rubbing and interlocking of the microstructure will occur.

For σ_1 in excess of 0.4 f_c (non-linear deformation regime), more and larger vertical microcracks are formed in the entire specimen volume, which leads to additional damage of the matrix and the interfaces between the matrix and aggregates (Fig. 9c). σ_1 is now mainly carried by the aggregates. This leads to an increase of the friction between aggregate–aggregate and aggregate–matrix, and a drastic increase of the energy dissipation during the pull-out of the grains from the aggregate interlock behind the crack tip. With increasing σ_1 loading, the "bridging" part of the fracture energy is increased and with it the total fracture energy (zone B in Fig. 9). The "microcracking" part decreases in this zone, but the amount of this decrease is overcompensated by the increase of the "bridging" part. This is verified by the smaller increase of the fracture energy in zone B with the smaller aggregates (MSA 16 and 8 mm) as compared to larger aggregates (32 mm MSA).

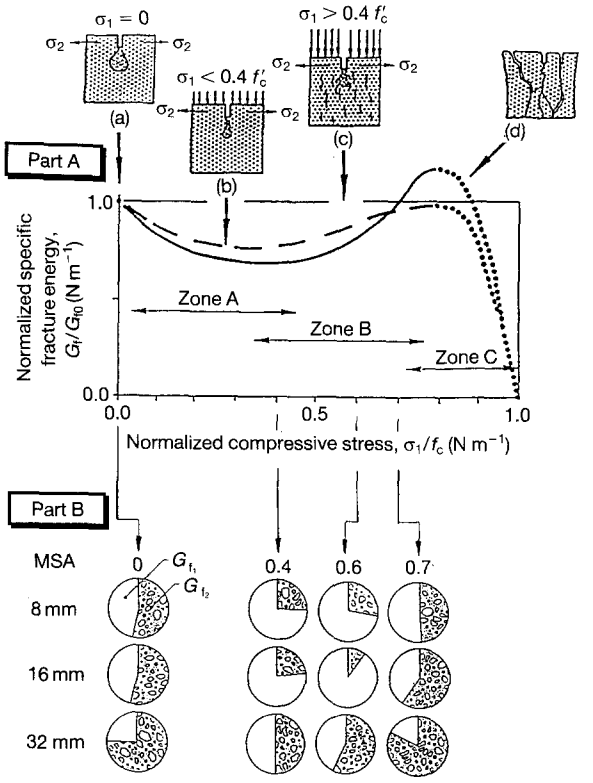

Figure 9 Fracture model for different σ_1 loadings: (– – –) 8 mm MSA; (——) 32 mm MSA. Part A: (a) $\sigma_1 = 0$, formation of unimpaired fracture process (FPZ), (b) constraint of FPZ due to σ_1, (c) increase of fracture energy due to friction and aggregate interlock in the microcracked material, (d) total failure lines refer to test extrapolation. Part B: distribution of two G_f portions related to "microcracking", G_{f_1}, friction and aggregate interlock "bridging", G_{f_2}, respectively.

If σ_1 is increased beyond 0.7–0.8 f_c, numerous cracks are formed (see schematic in Fig. 9d). The aggregate interlock loses its integrity which leads to a break down and disintegration of the microstructure.

If the measured load–displacement curves in Fig. 5 are considered in the light of this model, the following may be concluded: the lower peak at high σ_1 values (70% f_c) in comparison with lower σ_1 (25% f_c) may be explained by the fact that a high compressive load leads to pronounced microcrack formation and pre-damage forces in the ligament areas, so that crack initiation begins at lower splitting forces.

The different decay of the softening curve in the post-peak regime is a consequence of the higher "bridging" effect at higher σ_1 stresses. The apparent "higher ductility" in the decreasing part of the curve, seems to be caused by friction due to the aggregate–aggregate and aggregate–matrix interlock, which is more pronounced at high σ_1 stresses. Another consequence of this model is the fact that this mechanism is more effective in the case of large grains than of small ones.

6. Analytical evaluation

In a process to simulate numerically the G_f portions representing both microcracking and bridging, a data-fit program for load–displacement curves, SOFTFIT/FRACTURE I [28], was extended [29] to accommodate biaxial loading. SOFTFIT/FRACTURE, a widely used program, correlates interactively measured and calculated softening curves by minimizing the square root sum of squares between them. Starting with estimated values for f_1, s_1, w_1 and w_2, bilinear softening curves are developed using E-moduli of the test setup (concrete and steel) and the four parameters, Fig. 10. The four final values of f_1, s_1, w_1 and w_2 are considered material parameters, independent from specimen size and geometry. They can be used for arbitrary crack geometries and structural elements.

The main parameters resulting from the numerical analysis for selective softening diagrams, considered to be representative, are shown in Fig. 11. As an indicator for quality of compliance, measured versus calculated G_f values are added.

From this numerical evaluation, the above distinction between the two branches of the softening function is suggested, as discussed by several authors [26, 30], particularly [31]. It simulates the experimental results, namely that energy along the upper branch is

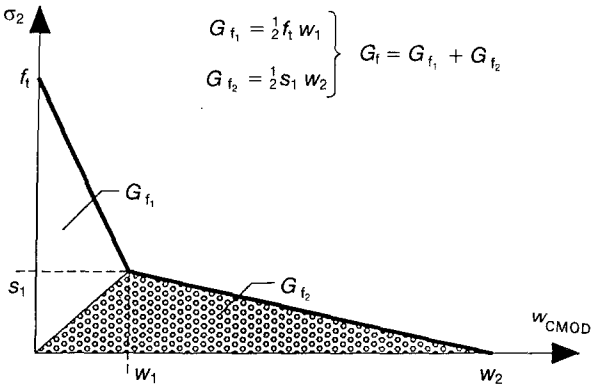

Figure 10 Bilinear softening diagrams and definition of the "microcracking", G_{f_1}, and "bridging", G_{f_2} part.

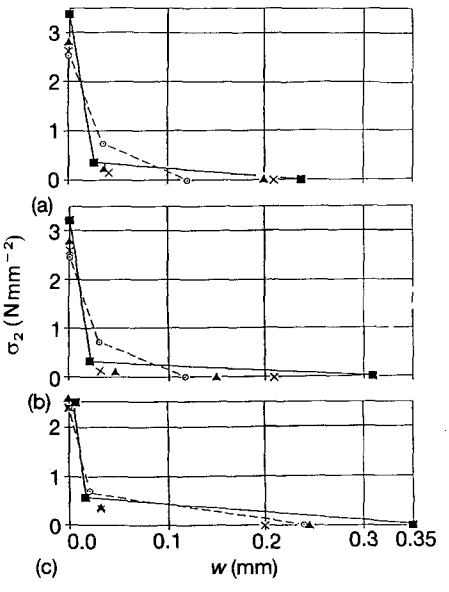

Figure 11 Result of numerical evaluation: bilinear softening diagrams for the three investigated concrete types: (a) 8 mm MSA (b) 16 mm MSA (c) 32 mm MSA. σ_1/f_c: (○) 0, (×) 0.4, (▲) 0.6, (■) 0.7.

dissipated by microcracking and along the lower branch by overcoming friction and tortuosity of aggregate interlock (bridging). Fracture energies related to these two phenomena are designated as G_{f1} and G_{f2} respectively in Figs 9 and 10.

Given this perspective one may conclude that σ_1 loading has a stabilizing influence on microcracking, or in other words: the preloading impedes lateral crack opening and propagation, confining it within a narrow FPZ. The material reacts more brittle and more energy is stored in the microcracked concrete. This is evident from both the steep first softening branches and the increase of G_{f1} for $0.6 > \sigma_1/f_c > 0$. Aggregate interlock increases with increasing MSA, Fig. 9b. This is valid for all σ_1 load cases.

These preliminary findings need further research. They may, however, be useful to formulate damage models, especially for assessing post-earthquake stability of massive concrete structures.

Finally it should be mentioned that the authors are aware of the unsolved size effect problem [32, 33] for both uniaxial and biaxial loading. This is to be studied on the basis of experience with loading equipments for a range of specimen dimensions.

7. Conclusions

Wedge splitting tests on 15 cm concrete cubes with three different MSAs under biaxial loading were conducted in order to get some insight into cracking under a tensile–compressive state of stress. Load–deformation diagrams for compressive stress levels, σ_1, between zero and 80% of the concrete's uniaxial compressive strength, f_c, were evaluated in terms of the specific fracture energy, G_f. The following can be concluded

1. The biaxial wedge splitting test arrangement, as developed by Tschegg, complies with the stipulated requirements, i.e. development of a uniform and well defined biaxial state of stress and stable load–deformation response over the entire range of loading. The test equipment is simple, easy to operate and inexpensive. Commonly available testing machines are sufficient for applying the test loads.

2. Uniaxial wedge splitting, $\sigma_1 = 0$ resulted in G_f values of 80 Nm^{-1} for MSA = 8 and 16 mm, and 110 Nm^{-1} for MSA = 32 mm. With increasing σ_1 loading G_f decreases within the elastic range of σ_1 and at the onset of microcracking (at σ_1 approximately 40% f_c) G_f starts to increase to a culmination point at around 70–80% f_c. This trend is more pronounced for the 32 mm than for the 8 and 16 mm concrete. Beyond this point total collapse of the material occurs.

3. With a simple model, Fig. 9, it is possible to explain the above unsteady development

(i) for $\sigma_1 = 0$ the FPZ can develop unimpeded;

(ii) for $0 < \sigma_1 < 0.4 f_c$ the FPZ is restrained, which leads to the reduction of G_f;

(iii) for $0.4 f_c < \sigma_1 < 0.8 f_c$ aggregate interlock and friction within the matrix is responsible for the rising branch; and

(iv) for $\sigma_1 > 0.8 f_c$, the material collapses.

4. A numerical simulation of the experimental results allowed splitting the fracture mechanism into energy release by microcracking and a subsequent bridging mechanism, thus confirming the above model.

It is therefore concluded that, in a tensile–compressive state of stress, a failure mechanism must be defined differently for the prepeak and post-peak branch of the stress–strain curve. This might influence the formulation of damage models, which is of practical significance, e.g. for the assessment of post-earthquake stability of mass concrete structures, such as dams.

Acknowledgements

The authors acknowledge the interest and support of Professor W. Wilk, President of the Technical Research & Advisory Institute of the Swiss Cement Industry, and thank the Austrian "Fonds zur Förderung der wissenschaftlichen Forschung" (FWF) which supported this study under project No. P8885-TEC.

References

1. H. KUPFER, H. K. HILSDORF and H. RÜSCHE, *J. Amer. Concr. Inst.* Aug. **8** (1969) 656.
2. H. KUPFER and K. H. GERSTLE, *J. Eng. Mech. Div. ASCE*, **99** (1973) 583.
3. L. J. M. NELISSEN, *HERON* **18** (1972) 1.
4. I. ROSENTHAL and J. GLUCKLICH, *J. Amer. Concr. Inst.* **11** (1970) 903.
5. K. H. GERSTLE *et al.*, *Proc. ASCE* **106** (1980) 1383.
6. M. D. KOTSOVOS and J. B. NEWMAN, *J. Amer. Concr. Inst.* Sept. **9** (1977) 443.
7. L. JIANG, J. L. HUANG, H. DAHAI and X. NIANXIANG, *J. Amer. Concr. Inst. Mater.* March–April **88** (1991) 181.
8. J. G. M. VAN MIER, *HERON* **31** (1986) 1.
9. *Idem, Materials and Structures. RILEM* **19**, (1986) 179.
10. A. J. ZIELINSKI, in "Fracture Toughness and Fracture Energy of Concrete", edited by F. H. Wittmann (Elsevier, Amsterdam, 1986) pp. 479–489.
11. J. WEERHEIJM, H. W. REINHARDT and S. POSTMA, in "Fracture Processes in Concrete, Rock and Ceramics", edited by J. G. M. van Mier, J. G. Rots and A. Bakker (Spon, London, 1991) pp. 839–848.
12. J. WEERHEIJM, PhD thesis, Delft University of Technology, 1992.
13. H. KREUZER, E. K. TSCHEGG and W. WILK, in "Proceedings of the International Conference on Dam Fracture", edited by V. Souma, R. Dungar and M. Moris, 11–13 September, Boulder, Co 1991 (Electric Power Research Institute, Palo Alto, CA, 1991) pp. 447–457.
14. E. K. TSCHEGG, H. KREUZER and M. ZELEZNY, in "Proceedings of the First International Conference on Fracture Mechanics of Concrete Structure", edited by Z. P. Bazant, 1–5 June, Breckenridge, CO, 1992 (Elsevier, London, 1992) pp. 455–460.
15. M. ELSER, MSc thesis 1991, Technical University, Vienna, Austria (in German).
16. RILEM draft recommendation (50-FMC), *Mater. & Struct.* **18** (1985) 287.
17. E. K. TSCHEGG, Patent AT No. 390328, patent application 31 January 1986 (in German).
18. *Idem*, Patent AT No. 396997, patent application, 4 January, 1990 (in German).
19. *Idem, Materialprüfung/Mater. Testing* **33** (1991) 338.
20. E. BRÜHWILER and F. H. WITTMANN, *Eng. Frac. Mech.* **35** (1990) 117.
21. Z. GUOFAN, JIAO HUI and X. SHILANG in "Fracture

Processes in Concrete, Rock and Ceramics", edited by J. G. M. van Mier, J. G. Rots and A. Bakker (Spon, London, 1991) pp. 789–798.
22. K. ROKUGO, M. IWASA, T. SUZUKI and W. KOYANAGI in "Fracture Toughness and Fracture Energy," edited by H. Mihashi H. Takahashi and F. H. Wittmann (Balkema, Rotterdam, 1989) pp. 153–163.
23. E. K. TSCHEGG, T. M. TAN and S. E. STANZL, *ASTM Testing & Eval. (submitted)*.
24. E. K. TSCHEGG, M. ELSER and S. E. STANZL-TSCHEGG, *Cement & Concr. Comp.* (submitted).
25. J. G. M. VAN MIER, *Cement & Concr. Res.* **1** (1991) 1.
26. M. KOTSOVOS and J. B. NEWMAN, *Concr. Res. (London)* **33** (1981) 103.
27. A. HILLERBORG, A. MODEER, and P. E. PETERSON, *Cement & Concr. Res.* **16** (1976) 773.
28. P. E. ROELFSTRA, PhD thesis, Ecole Polytechnique Federale de Lausanne, Lausanne, 1988.
29. *Idem*, Private communication, 1991.
30. T. C. HSU, G. M. STURMAN and G. WINTER, *Proc. Amer. Concr. Inst.* **60** (1962) 209.
31. N. NOMURA, H. MIHASHIE and M. IZUMI, in "Fracture Processes in Concrete, Rock and Ceramics", edited by J. G. M. van Mier, J. G. Rots and A. Bakker (Spon, London, 1991) pp. 51–60.
32. P. ZDENEK and P. BAZANT, *J. Eng. Mech.* **110** (1984) 518.
33. H. K. HILSDORF and W. BRAMESHUBER, "Baustoffe" (Bauverlag, Wiesbaden, 1985) pp. 62–72.

Received 6 September 1993
and accepted 5 May 1994